Mechanical Engineering Advances 2024, 2(1), 526.
https://doi.org/10.59400/mea.v2i1.526

Article

First and second law analysis of crack propagation in canvas painting

Mohammad Yaghoub Abdollahzadeh Jamalabadi

Faculty of Marine Engineering, Chabahar Maritime University, Chabahar 99717-56499, Iran; my.abdollahzadeh@cmu.ac.ir

CITATION

Jamalabadi MYA. First and second law analysis of crack propagation in canvas painting. 2024; 2(1): 526. https://doi.org/10.59400/mea.v2i1.526

ARTICLE INFO

Received: 30 January 2024
Accepted: 24 February 2024
Available online: 2 April 2024

Abstract: The knowledge of how the craquelures happen and their pattern on historical objects, especially paintings, is interested in the field of cultural heritage. Entropy generation and thermal analysis of crack growth are calculated numerically for the canvas painting. The painting is modeled as a three-layer composite with isotropic material properties. An in-house code is developed to model the plane strain elasto-static structural mechanics with hybrid-Trefftz finite element formulation. The results are benchmarked with numerical and analytical solutions. Entropy generation and temperature fields are simulated throughout stacking in mode I of a delamination process. The parameter study shows that the parameter of entropy has a great influence on the process of expectation of break proliferation in fast and low areas. It is likewise demonstrated that the use of the corruption entropy age hypothesis gives a technique for assessing the steady in the law of crack growth regarding the rate of entropy production.

Keywords: crack growth; thermodynamic analysis; entropy production; fatigue; thermal balance

1. Introduction

Almost all mechanical parts encountering cyclic stacking are helpless to building up a crack(s) that will in general proliferate and inevitably cause break disappointment, frequently abruptly and with calamitous outcomes. In this manner, it is nothing unexpected that numerous endeavors have been made to comprehend the idea of break development with cyclic stacking to prepare for crack. The stress intensity factor was created in 1957 by George R. Irwin, the man typically viewed as the first author of crack mechanics [1]. The stress intensity factor (K_I) for applied stress σ and crack length a is

$$K_I = \sigma F \sqrt{\pi a} \tag{1}$$

where F is a function of geometry.

When all is said and done, an article can be stacked toward any path comparative with a break. The sketch at the right shows a power vector in such an arbitrary direction. It is for the most part opposite to the split, yet additionally contains segments that produce in-plane and out-of-plane shear. At the point when this happens, the consistent activity is parceling the power into its basic segments. This procedure prompts the three stacking modes demonstrated as follows: Mode I loading happens frequently and produces the most harm. Along these lines, it normally gets the most consideration in examine, basic structure, disappointment investigation, and so forth. It is usually called the opening mode. Mode II corresponds to shearing of the broken face due to in-plane shear stresses. It presumably gets the second most consideration because the issue is as yet 2-D since all the activity is in-plane. Mode II stacking impacts split development heading in a manner that limits further Mode II stacking

while at the same time boosting Mode I. Mode III is the Tearing Mode for clear reasons. It is driven by out-of-plane shear pushing and doesn't appear to happen as regularly as the other two.

It is one of the most basic and valuable parameters in all of crack mechanics. The pressure force factor portrays the pressure state at a broken tip, is identified with the pace of split development, and is utilized to set up disappointment criteria because of crack. After two decades, Irwin indicated that Westergaard's outcome could be incredibly streamlined in the territory promptly encompassing the broken tip. He did as such by communicating in the district close to the broken tip. This disparity was utilized by Irwin to discover straightforward articulations (well, contrasted with the perplexing capacities). Irwin's improvement halted here, and this is for sure the characteristic spot to stop. In any case, in the years following Irwin's distribution, it got well known to incorporate. The two conditions have appeared in the diagram underneath. Unmistakably both are extremely close at the split-tip and wander as the good ways from the tip increments. The district of close understanding is roughly one may ask, why even waste time with Irwin's exact arrangement when Westergaard's accurate arrangement is accessible? There are a few reasons. In the first place, the estimated arrangement is, in fact, precise at the broken tip, and this is all that truly matters because the conditions at the split-tip direct (i) how quick the break develops, (ii) in which course it develops, and (iii) regardless of whether it flops disastrously. Second, the inexact arrangement uncovers the reliance of the pressure parts on totally depicting the seriousness of the pressure state at the split tip. Irwin perceived this and first utilized the term pressure force factor to depict the articulation.

Hypothetical models that use continuum harm mechanics essentially center around the debasement of the material before the commencement of a smaller scale break. Among outstanding commitments on the evaluation of split proliferation is the old-style work [1], which utilized the pressure power factor to land at an experimental connection for measuring the break spread. Other researchers adjusted the supposed by thinking about the impact of the average tension. Break conclusion impact was presented to portray the distinction between the consistency of the broken structure in airplane solid parts exposed to various loads.

When all is said and done, weakness in solids develops in 4 phases. The main phase includes the settlement or phase arrangement where separations happen and lasting groups are framed [2]. In the subsequent phase, separations to smaller-scale splits happen [3], and, in the third stage, the miniaturized scale breaks will, in general, arrange themselves opposite to the heading of greatest average pressure. A break is then shaped, and as it gets larger, it produces stress focused at the crack point. The last phase of exhaustion harm includes the spread of the large-scale break, described by striation and seashore mark development [4]. A large scale split quickly engenders until the last crack.

From the material's perspective, the development and proliferation of a visible crack are related to zone arrangement in front of the broken focus. The study right now is a wellspring of warmth age. The part of the plastic area changed over volume relies upon a few factors, for example, the yield strain, plastic strain, and strain solidifying. Research shows that 0.8 and 0.95 of work is changed to heat [5,6]. All the more, as of late, thermographic estimation systems have been utilized to increase further

knowledge into the idea of break spread. For instance, Breen et al. [7] utilized vitality scattering to break down weakness conduct in tempered steel. Other researchers [8] gave results to titanium combinations notwithstanding hardened steel. On the other hand

Chen et al. [9] revealed the spread of power esteems and demonstrated that versatile impact is prevailing in circumstances of average stress [10].

The thickness of cracks, direction (isotropy or anisotropy to grain), its change (smooth or jagged), square island frequency, and network (junctions, random) are the problems. For example, Italian has jagged cracks with a predominant direction, perpendicular to grain [11–14]. While Flemish straight cracks are parallel to grain with very small smooth islands. As well, Dutch cracks are jagged perpendicular to the longest side with medium-sized islands, but French curved cracks have no predominant direction with large smooth islands.

In old paintings, breaks of molecular bonds cause disorder in the network and cracks [15]. The painting film thickness plays a great role in crack propagation and the final geometry of each pattern [16]. As cracks of lateral area are powered by bulk stress energy, the critical force is related to film thickness and overcrack area to the power of 3/4 (see Equation (4) in Lazarus and Pauchard [16]). They found a relation between the average number of polygons and an analogy thermodynamic micro-canonical entropy. Another study [17] based on the porosity of the cement substrate on building coating shows that the change in entropy of the system causes greater defectiveness (probability of destruction). The entropic endurance level at the time crack initiation is measured in Karimian et al. [18]. They propose the entropy method to predict crack initiation. Entropy in crack networks in old paintings with saturation prospectus analyzed in other references [15,19–24]. Jamalabadi et al. [25–28] suggested that substrate material responsiveness to variations in relative humidity is the most dangerous condition for cracking a panel painting.

In the present paper, the plane strain electrostatic structural mechanics with hybrid-Trefftz finite element formulation [21] is used to model cracks in paintings. The numerical and analytical solutions are used to validate the used method. Entropy generation and temperature fields are simulated during cyclic loading on painting. The parameter study is used to study the entropy production rate.

2. Mathematical model

2.1. Second low analysis (entropy generation) in fatigue

Deformation is when an object changes its shape or size because of temperature or force. There are two types of energy release through fatigue: elastic deformation energy and plastic deformation energy. Elastic deformation is reversible, like when someone stretches a rubber band and it goes back to its original shape. Plastic deformation is irreversible, like when someone bends a steel rod and it stays bent even after letting it go. In the field of thermodynamics, fatigue damage is considered a process that cannot be reversed, and it releases energy, resulting in the creation of entropy. This irreversible process and the generation of entropy can be quantified by measuring the amount of thermal, strain, and acoustic energies that are dissipated when a system undergoes fatigue. The entropy generated through the fatigue process

at the absolute temperature of T, heat flux, and temperature gradients of ∇T calculated by summation of three components of plastic work, heat conduction, and thermodynamic work as

$$\dot{S_g} = \frac{W_p}{T} - \frac{\nabla T}{T^2} J_q - \frac{1}{T} A_k \dot{v_k} \tag{2}$$

where $A_k \dot{v_k}$ is the thermodynamic works consist of the state internal variables relating to irreversible deformation mechanisms (cyclic hardening/softening, phase transformation, surface traction, body force, and the so-called micro-forces, etc.), $\dot{v_k}$ and the conjugate thermodynamic forces associated with them A_k, and the plastic work W_p is defined as multiplication of stress tensor σ and plastic strain rate tensor $\dot{\varepsilon_p}$ as

$$W_p = \sigma : \dot{\varepsilon_p} \tag{3}$$

The amount of energy forces in a system depends on its current thermodynamic state, while the dissipative forces only depend on the rate at which the system changes. Interestingly, in a quasi-static setting where the system's velocities decrease, the dissipative forces should disappear. The second and third terms are neglected in common engineering problems, and Equation (1) is simplified. Total fatigue fracture entropy, can be evaluated by integrating non-negative entropy generation of Equation (2) from time $t = 0$ to $t = t_f$, when fracture occurs:

$$S_g = \int_0^{t_f} \frac{W_p}{T} dt \tag{4}$$

That value could be evaluated from a pure material such as stainless steel with properties given in **Table 1**. The rate of strain can be calculated from

$$\frac{\Delta \epsilon}{2} = \frac{\Delta \sigma}{2E} + \alpha \left(\frac{\Delta \sigma}{2k'} \right)^{1/n'} \tag{5}$$

Table 1. Mechanical properties of stainless steel 304.

parameter	**value**
E (GPa)	193
μ (GPa)	79
k (W/mK)	16.3
n'	0.26
k' (MPa)	1200
λ (m^2/s)	4.06×10^{-6}
t (mm)	1.85
σ_0 (MPa)	270

where the Stress Coefficient k', Strain Coefficient α and Exponential Coefficient constants n' for each layer are given in **Table 2**.

$$\Delta \sigma_{ij} = \Delta \sigma_0' \left(\frac{\Delta K_I^2}{\alpha \Delta \sigma_0'^2 I_{n'} r} \right)^{\frac{n'}{n'+1}} \tilde{\sigma}_{ij}(n', \theta) \tag{6}$$

Table 2. Mechanical properties of three layer painting on canvas.

parameter	value
E (MPa)	38.6
α (1/°C)	10^{-5}
v	0.3
t (mm)	0.152
glue	
E (GPa)	3.791
α (1/°C)	2.5×10^{-5}
v	0.3
t (mm)	0.0508
Naples yellow oil paint	
E (GPa)	0.327
α (1/°C)	5.2×10^{-5}
v	0.3
t (mm)	0.152

Finally, the term needed for Equation (4) for the dissipated energy can be determined using the following equation

$$W_p = f\left(\frac{1-n^{'}}{1+n^{'}}\right)\sigma_{eq}\varepsilon_{eq}^{p} \tag{7}$$

For plane stress the angle θ dependency of stress factor variation ΔK_I comes form

$$\omega(\theta) = \frac{1}{16\pi}\frac{\Delta K_I^2}{\sigma_0^{'2}}\left(1+\frac{3}{2}sin^2\theta + cos\theta\right) \tag{8}$$

and plane strain the angle dependency of stress factor comes form

$$\omega(\theta) = \frac{1}{16\pi}\frac{\Delta K_I^2}{\sigma_0^{'2}}\left((1-2v)^2(1+cos\theta) + \frac{3}{2}sin^2\theta\right) \tag{9}$$

the cyclic BC is used. Since for horizontal line plane stress is

$$\omega_0 = \frac{1}{8\pi}\frac{\Delta K_I^2}{\sigma_0^{'2}} \tag{10}$$

and plane strain is

$$\omega_0 = \frac{1}{8\pi}\frac{\Delta K_I^2}{\sigma_0^{'2}}(1-2v)^2 \tag{11}$$

2.2. First low analysis (thermal balance) in fatigue

Temperature field near crack zone is

$$\frac{\rho C}{k}\frac{\partial T}{\partial t} = \nabla^2 T + \frac{q}{k} \tag{12}$$

where q is the heat generation rate comes from plastic form in Equation (7) and in Cartesian coordinates the Laplacian operator is:

$$\nabla^2 = \frac{\partial^2}{\partial x^2} + \frac{\partial^2}{\partial y^2} \tag{13}$$

The dissipated energy from the crack tip in the plastic zone as a function of cycle number is

$$\frac{dw_p}{dN} = At\frac{(\Delta K_I)^4}{\mu\sigma_0^2} \tag{14}$$

where t is the thickness and A is constant

2.3. Trefftz triangular finite element for linear elasticity

For a dimensional static linear elasticity problem defined in the domain Ω and boundaries (displacement boundaries Γ_u and traction boundaries Γ_t) presented in **Figure 1**, the governing equation is given by:

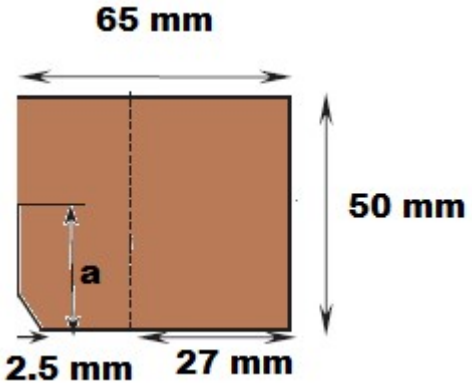

Figure 1. The experimental setup.

$$\ddot{\rho u} = \nabla \cdot \sigma + f \tag{15}$$

with the following boundary conditions presented in Figure\ref {FIG:3}:

$$u = \overline{u}\ on\ \Gamma_u \tag{16}$$

And

$$\sigma \cdot \boldsymbol{n} = \bar{\boldsymbol{t}}\ on\ \Gamma_t \tag{17}$$

The discrete equations for this problem formulated from Galerkin weak form of the governing Equation (15) is given by:

$$\int_{\Omega} (\nabla u)^T D(\nabla \delta u) d\Omega - \int_{\Omega} (\delta u)^T b d\Omega - \int_{\Gamma_t} (\delta u)^T \bar{\boldsymbol{t}} d\Gamma = \mathbf{0} \tag{18}$$

where u and δu are the trial and the test functions, respectively, and is the material constitutive matrix. The FEM uses the same trial and test functions. The finite element expansion of the governing equation, which is the series of the homogeneous solution, is given by:

$$u(x) = \sum_i N_i(x) c_i \tag{19}$$

Since the displacement matrix can be approximated by shape functions $N_i(x)$ with nodal degrees of freedom c_i which leads to the discretized algebraic system of equations:

$$\ddot{Mu} + Ku = F \tag{20}$$

In Equation (20), M denotes the elastic inertia matrix, K denotes the elastic rigidity matrix, F denotes the external body force matrix, and u is the displacement

matrix, which they calculated in detail by

$$M = \int_{\Omega} N^T DN d\Omega \tag{21}$$

for the elastic inertia matrix and elastic rigidity matrix

$$K = \int_{\Omega} B^T DB d\Omega \tag{22}$$

The stiffness matrix is computed over each element and assembled to the global matrix. The size of the stiffness matrix depends on the number of nodes in an element. and external body force matrix

$$\boldsymbol{f} = \int_{\Omega} N^T b d\Omega + \int_{\Gamma_t} N^T \bar{\boldsymbol{t}} d\Gamma \tag{23}$$

3. Results

The thermal field spiral bearing is evaluated within the Fourier arrangement with four introductory expansions. The schematic is shown in **Figure 1**. This figure illustrates the setup used for conducting the experiment. It may show the equipment, instruments, or apparatus used in the study. Convergence is presented in **Table 3**. The method of three reference stress intensity factors leads to weight functions. Table 1 shows the mechanical properties of stainless steel 304. The loading cycle is 20 Hz. Material SS 304 is used for validation, as shown in **Figure 2**. This figure presents the comparison between the growth rate of a crack and the amount of entropy generated using experimental data. It helps validate the relationship between crack growth and entropy generation. In **Figure 2**, the spread appropriation of entropy generation around crack tip and crack speed is presented. **Figure 2** shows the break proliferation velocity taken from **Table 1**.

Table 3. Grid study.

Mesh number	Relative Error
783	0.02
4325	0.007
48210	0.003
81034	0.0005
128301	0

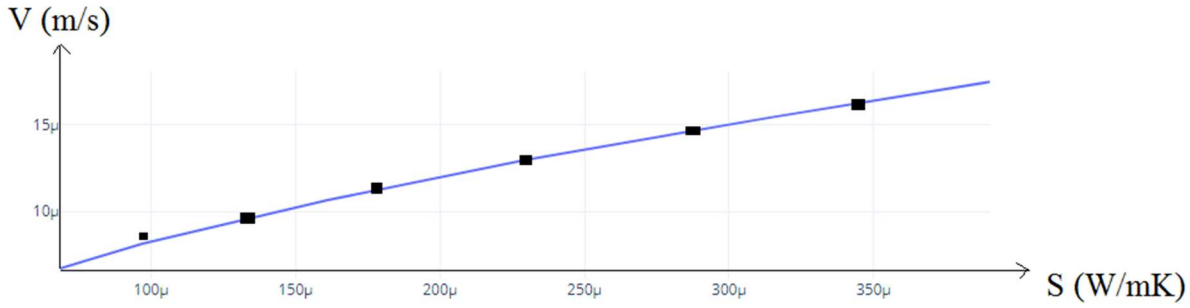

Figure 2. Validation of growth rate of crack versus entropy generation with experimental data.

As shown in **Figure 2**, the velocity of crack propagation increased with an increase in entropy generation around the crack tip.

Schematics of three-layer painting on canvas are presented in **Figure 3**. Note that the decision of the estimation of Fm is with the end goal that the outer pressure applied by the tip, Fm/S (being the anticipated surface of the tip on the film), is near the fine weight applied by the air/dissolvable meniscus at the dissipation surface of the layer. This figure provides a visual representation or diagram of the process or structure involved in a three-layer painting technique on canvas. It may show the layers and their arrangement.

Figure 3. Schematics of three layers painting on canvas.

In **Figure 4**, the distribution of shear stress and normal stress in painting layers are presented. This figure displays the distribution or magnitude of stress within a three-layer painting on canvas. It helps visualize the impact of the layers on the stress distribution. Warmth age of roundabout area split through the range of crack tip. **Figure 4** shows the engendering speed as an element of warmth age. The chart shows the consequences of the four tests. In ordinary exhaustion split engendering, the spread is examined in a moderately that conceivable to plan as indicated by the pressure power factor. Results displayed right now stream as a decent marker at low spread rates.

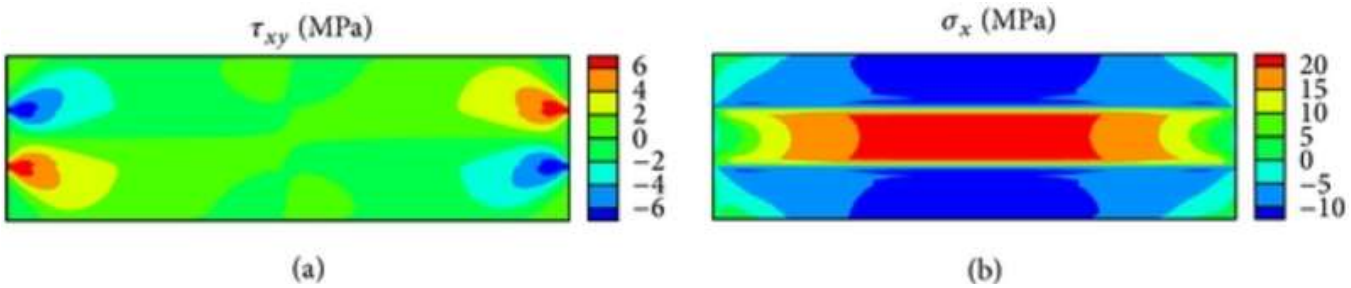

Figure 4. Stress in three layers painting on canvas.

In **Figure 5**, the thermal field in painting layers is presented. This figure depicts the thermal field or temperature distribution within a three-layer painting on canvas. It shows how heat is distributed across the layers and can provide insights into the painting process. To show the upside of utilizing entropy age in break spread examination, **Figure 5** delineates the examination between proliferation within the component of force stream. As appeared in **Figure 6**, the pressure power can't anticipate the speed; however, the entropy age approach yields reliable outcomes in

every one of the areas. It is viewed as a quick proliferation.

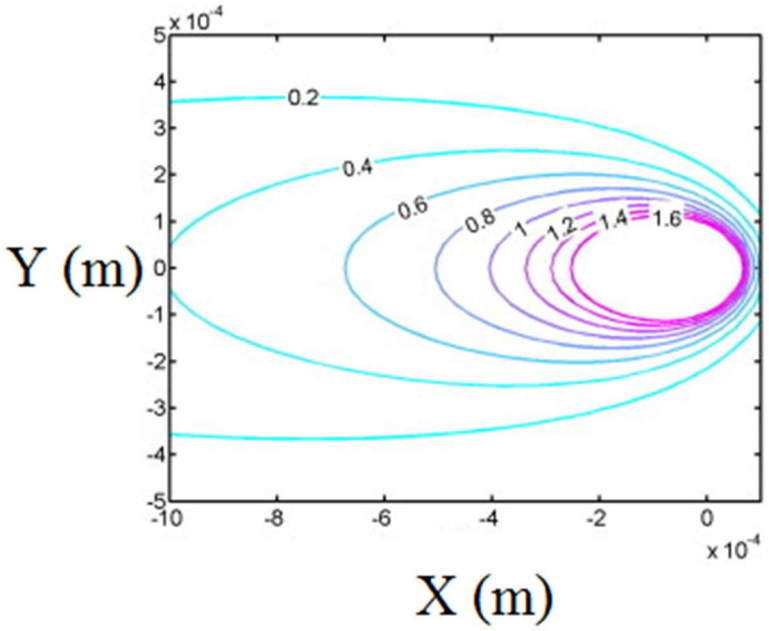

Figure 5. Increase of temperature (K) in three layers painting on canvas.

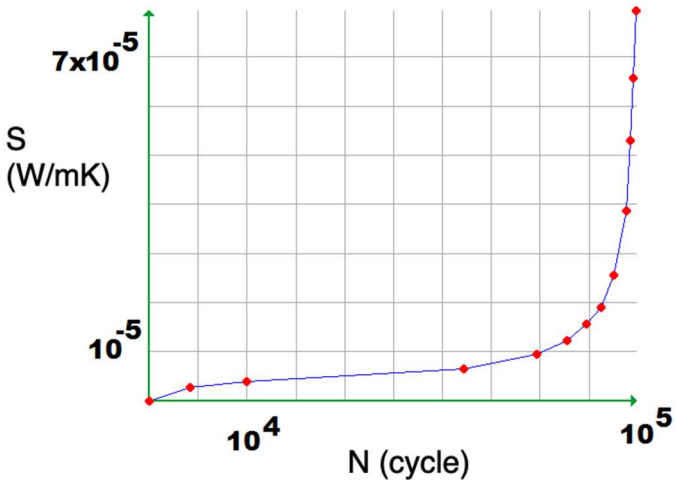

Figure 6. Entropy production versus cycle.

Entropy creation (or production) is the measure of entropy that is delivered in any irreversible procedures, for example, warmth and mass exchange forms, including the movement of bodies, heat trade, liquid stream, substances growing or blending, anaplastic distortion of solids, and any irreversible thermodynamic cycle. Entropy production versus cycle is presented in **Figure 6**. This figure plots the relationship between entropy production and the number of cycles or repetitions in a process. It helps analyze the change in entropy with each cycle.

Paris-Erdogan law (equation for rate of fatigue crack growth) is formulated by stress intensity factor and loading cycle. Based on crack growth versus entropy generation, the crack length can be predicted. Crack length rate versus entropy is presented in **Figure 7**. Split proliferation happens when the vitality stream from the pressure strain field to the break edge locale is adequate for supporting the procedures prompting mixtures of miniaturized scale partitions with the principle split. This figure

illustrates the relationship between the rate of crack lengthening and the amount of entropy generated. It helps understand how crack growth is related to entropy in the system. The investigation of the vitality stream to the procedure district is somewhat confounded in the general case.

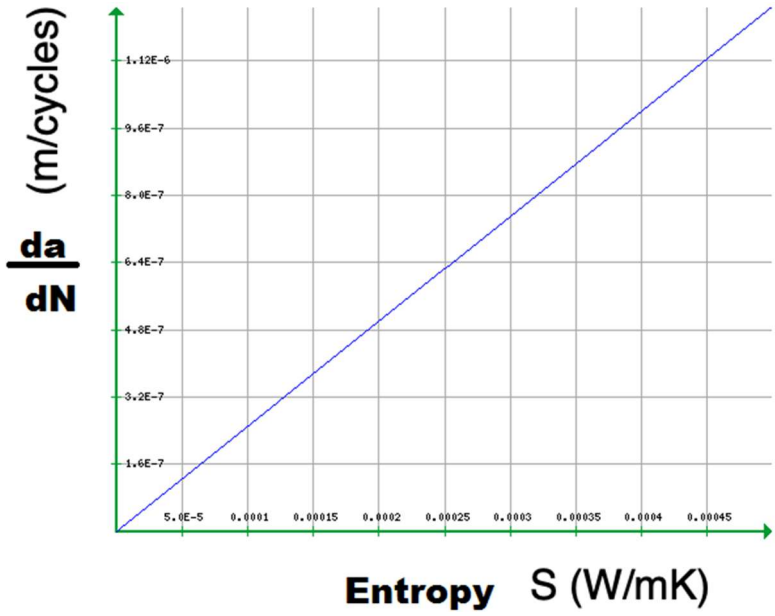

Figure 7. Crack length rate versus entropy.

4. Conclusion

The knowledge of how the craquelure happens and their pattern on historical objects, especially paintings, is interested in the field of cultural heritage. Entropy generation and thermal analysis were calculated numerically for the canvas painting. The painting is modeled as a three-layer composite with isotropic material properties. A house code is developed to model the plane strain elastostatic structural mechanics with hybrid-Trefftz finite element formulation. The results are benchmarked with numerical and analytical solutions. The main results are:

1) In mode, entropy generation and temperature field are simulated stacking of a delamination process.
2) The entropy generation parameter was significant in the expectation of break proliferation growth in fast areas.
3) It is likewise demonstrated that the use of the corruption entropy age hypothesis gives a technique for assessing the steady in Paris law regarding entropy production rate.

Conflict of interest: The author declares no conflict of interest.

References

1. Bueckner HF. Novel principle for the computation of stress intensity factors. Zeitschrift fuer Angewandte Mathematik & Mechanik. 1970; 50: 129-146.
2. Rice J. Some remarks on elastic crack-tip stress field. International Journal of Solids and Structures. 1972; 8: 751-758. doi: 10.1016/0020-7683(72)90040-6

3. Baraff D, Witkin A. Large steps in cloth simulation. In: Proceedings of the 25th Annual Conference on Computer Graphics and Interactive Techniques—SIGGRAPH'98; 18-24 July 1998; Orlando, USA. doi: 10.1145/280814.280821
4. Berger GA, Russell WH. Deterioration of Surfaces Exposed to Environmental Changes. Journal of the American Institute for Conservation. 1990; 29(1): 45-76. doi: 10.1179/019713690806046145
5. Blinn JF. Simulation of wrinkled surfaces. In: Proceedings of the 5th Annual Conference on Computer Graphics and Interactive Techniques; 23-25 August 1978; Atlanta, Georgia, USA. doi: 10.1145/800248.507101
6. Blinn JF, Newell ME. Texture and reflection in computer generated images. Communications of the ACM. 1976; 19(10): 542-547. doi: 10.1145/360349.360353
7. Breen DE, House DH, Wozny MJ. Predicting the drape of woven cloth using interacting particles. In: Proceedings of the 21st Annual Conference on Computer Graphics and Interactive Techniques—SIGGRAPH'94; 24-29 July 1994; Orlando, Florida, USA. doi: 10.1145/192161.192259
8. Carignan M, Yang Y, Thalmann NM, et al. Dressing animated synthetic actors with complex deformable clothes. ACM SIGGRAPH Computer Graphics. 1992; 26(2): 99-104. doi: 10.1145/142920.134017
9. Chen Y, Lin S, Hua Z, et al. Realistic rendering and animation of knitwear. IEEE Transactions on Visualization and Computer Graphics. 2003; 9(1): 43-55. doi: 10.1109/tvcg.2003.1175096
10. Cook RL. Shade trees. In: Proceedings of the 11th Annual Conference on Computer Graphics and Interactive Techniques; 23-27 July 1984; Minneapolis, Minnesota, USA. doi: 10.1145/800031.808602
11. Cook RL, Carpenter L, Catmull E. The Reyes image rendering architecture. In: Proceedings of the 14th Annual Conference on Computer Graphics and Interactive Techniques; 27-31 July 1987; Anaheim, California, USA. doi: 10.1145/37401.37414
12. Corel. Painter® Essentials 7 Quick Start Guide. Available online: https://product.corel.com/help/Painter-Essentials/540223061/Main/EN/Quick-Start-Guide/Painter-Essentials-Quick-Start-Guide.pdf (accessed on 12 January 2024).
13. Daubert K, Seidel HP. Hardware-Based Volumetric Knit-Wear. Computer Graphics Forum. 2002; 21(3): 575-583. doi: 10.1111/1467-8659.t01-1-00708
14. Daubert K, Lensch HPA, Heidrich W, Seidel H-P. Efficient cloth modeling and rendering. In: Proceedings of the 12th Eurographics Workshop on Rendering Techniques; 25-27 July 2001; London, UK.
15. Flores JC. Entropy Signature for Crack Networks in Old Paintings: Saturation Prospectus. Entropy. 2018; 20(10): 772. doi: 10.3390/e20100772
16. Lazarus V, Pauchard L. From craquelures to spiral crack patterns: influence of layer thickness on the crack patterns induced by desiccation. Soft Matter. 2011; 7(6): 2552. doi: 10.1039/c0sm00900h
17. Loganina V, Fediuk R. Thermodynamic Approach to Assessing the Curing of Protective and Decorative Coatings of Exterior Walls of Buildings. Materials Science Forum. 2019; 974: 3-8. doi: 10.4028/www.scientific.net/msf.974.3
18. Karimian SF, Bruck HA, Modarres M. Thermodynamic entropy to detect fatigue crack initiation using digital image correlation, and effect of overload spectrums. International Journal of Fatigue. 2019; 129: 105256. doi: 10.1016/j.ijfatigue.2019.105256
19. Flores JC, Palma-Chilla L. Entropy behavior for isolated systems containing bounded and unbounded states: latent heat at the inflection point. Journal of Physics Communications. 2020; 4(3): 035002. doi: 10.1088/2399-6528/ab78df
20. Agarwal N, Farris RJ. Thermodynamics of deformation of latex blend coatings and its implications for tailoring their properties. Journal of Coatings Technology. 1999; 71(9): 61-72. doi: 10.1007/bf02698385
21. Hirshikesh, Natarajan S, Annabattula RK, et al. Trefftz polygonal finite element for linear elasticity: convergence, accuracy, and properties. Asia Pacific Journal on Computational Engineering. 2017; 4(1). doi: 10.1186/s40540-017-0020-3
22. Ostoja-Starzewski M. Crack patterns in plates with randomly placed hole: A maximum entropy approach. Mechanics Research Communications. 2001; 28: 193-198. doi: 10.1016/S0093-6413(01)00162-8
23. Hajshirmohammadi B, Khonsari MM. Thermographic evaluation of metal crack propagation during cyclic loading. Theoretical and Applied Fracture Mechanics. 2020; 105: 102385. doi: 10.1016/j.tafmec.2019.102385
24. Hajshirmohammadi B, Khonsari MM. On the entropy of fatigue crack propagation. International Journal of Fatigue. 2020; 133: 105413. doi: 10.1016/j.ijfatigue.2019.105413
25. Abdollahzadeh Jamalabadi MY. Optimal rectangular crack pattern based on constructal, fracture saturation, and energy minimization theories for painting on wood. Chaos, Solitons & Fractals. 2022; 160: 112242. doi: 10.1016/j.chaos.2022.112242
26. Abdollahzadeh Jamalabadi MY. The Use of Artificial Intelligence for Image Processing of Crack Patterns in Panel Painting.

Sumerianz Journal of Scientific Research. 2022; 51: 1-12. doi: 10.47752/sjsr.51.1.12

27. Mohammad Yaghoub AJ. Paintings crack initiation time caused by microclimate. Annals of Mathematics and Physics. 2021; 4(1): 92-101. doi: 10.17352/amp.000028
28. Abdollahzadeh Jamalabadi MY, Zabari N, Bratasz Ł. Three-dimensional numerical and experimental study of fracture saturation in panel paintings. Wood Science and Technology. 2021; 55(6): 1555-1576. doi: 10.1007/s00226-021-01328-z